Research Article / *Araştırma Makalesi*

Ege Journal of Medicine / *Ege Tıp Dergisi* 2026; 65 (3): 507-518

Development of an extracellular vesicle-based shRNA delivery system to overcome cisplatin resistance in non-small cell lung cancer by targeting STAT3

Küçük hücreli olmayan akciğer kanserinde sisplatin direncini aşmak için hücre dışı vezikül tabanlı STAT3'ü hedefleyen shRNA taşıyıcı sistemin geliştirilmesi

Mustafa Kotmakci[1] Vildan Bozok[2]

[1]Department of Pharmaceutical Biotechnology, Faculty of Pharmacy, Ege University, İzmir-Türkiye

[2]Ege University Faculty of Medicine, Department of Medical Biology, İzmir-Türkiye

ABSTRACT

Aim: Cisplatin resistance remains a major clinical challenge in non-small cell lung cancer, frequently driven by STAT3 activation. This study aimed to engineer an autologous extracellular vesicle (EV) formulation loaded with anti-STAT3 shRNA-encoding plasmid DNA to resensitize cisplatin-resistant Calu1 lung cancer cells.

Materials and Methods: EVs were isolated from parental Calu1 cell culture supernatants via modified differential ultracentrifugation and characterized using electron microscopy, atomic force microscopy, and dynamic light scattering. Plasmid DNA was loaded into EVs via lipofection-mediated membrane fusion. Formulation integrity and protection were assessed using agarose gel electrophoresis and a DNase I assay. *In vitro* cytotoxicity, STAT3 knockdown, and cisplatin resensitization were evaluated in a cisplatin-resistant subline (CR-Calu1) using WST-1 viability assays, RT-qPCR, and Western blot analysis.

Results: Isolated EVs displayed characteristic spherical morphology and a typical size distribution. The biomimetic formulation successfully encapsulated the pDNA, conferring robust protection against DNase I degradation. In CR-Calu1 cells, pshSTAT3-loaded EVs significantly downregulated STAT3 mRNA expression (48–58% reduction) and correspondingly decreased protein levels. Crucially, combining these EVs with sub-lethal cisplatin doses synergistically reduced cell viability compared to cisplatin alone, effectively restoring chemosensitivity. Stability optimization identified 7.5% glycine as the superior cryoprotectant, maintaining EV structural integrity post-lyophilization.

Conclusion: We successfully engineered a stable, lyophilizable EV-based gene delivery platform. Targeting STAT3 via this autologous system effectively reverses acquired drug resistance, representing a viable therapeutic strategy for refractory NSCLC.

Keywords: *Cisplatin resistance, extracellular vesicles, exosome, NSCLC, STAT3*

ÖZ

Amaç: *Sisplatin direnci, genellikle STAT3 aktivasyonu tarafından yönlendirilen, küçük hücreli dışı akciğer kanserinde (KHDAK) önemli bir klinik zorluk olmaya devam etmektedir. Bu çalışma, sisplatine dirençli Calu1 akciğer kanseri hücrelerini yeniden duyarlı hale getirmek için anti-STAT3 shRNA kodlayan plazmit DNA yüklü otolog bir ekstraselüler vezikül (EV) formülasyonu tasarlamayı amaçlamıştır.*

Gereç ve Yöntem: *EV'ler, modifiye edilmiş diferansiyel ultrasantrifügasyon yoluyla atasal Calu1 hücre kültürü süpernatantlarından izole edildi ve elektron mikroskobu, atomik kuvvet mikroskobu ve dinamik ışık saçılımı kullanılarak karakterize edildi.*

Corresponding author: Mustafa Kotmakci
Department of Pharmaceutical Biotechnology, Faculty of Pharmacy, Ege University, Izmir-Türkiye
E-mail: *mustafa.kotmakci@ege.edu.tr*
Application date: 18.05.2026 Accepted: 15.06.2026

Plazmit DNA, lipofeksiyon aracılı membran füzyonu ile EV'lere yüklendi. Formülasyon bütünlüğü ve koruması, agaroz jel elektroforezi ve bir DNaz I analizi kullanılarak değerlendirildi. İn vitro sitotoksisite, STAT3 susturulması ve sisplatin yeniden duyarlılaştırması, WST-1 canlılık testleri, RT-qPCR ve Western blot analizi kullanılarak sisplatine dirençli bir alt seride (CR-Calu1) değerlendirildi.

Bulgular: *İzole edilen EV'ler karakteristik küresel morfoloji ve tipik bir boyut dağılımı sergiledi. Biyomimetik formülasyon, pDNA'yı başarıyla enkapsüle ederek DNaz I bozunmasına karşı güçlü koruma sağladı. CR-Calu1 hücrelerinde, pshSTAT3 yüklü EV'ler STAT3 mRNA ekspresyonunu anlamlı ölçüde aşağı regüle etti (%48–58 azalma) ve buna bağlı olarak protein seviyelerini düşürdü. Kritik olarak, bu EV'lerin subletal sisplatin dozlarıyla birleştirilmesi, yalnızca sisplatine kıyasla hücre canlılığını sinerjistik olarak azalttı ve kemosensitiviteyi etkili bir şekilde geri kazandırdı. Stabilite optimizasyonu, liyofilizasyon sonrası EV yapısal bütünlüğünü koruyan üstün kriyoprotektan olarak %7,5 glisini belirledi.*

Sonuç: *Stabil, liyofilize edilebilir bir EV tabanlı gen taşıma platformunu başarıyla tasarladık. Bu otolog sistem aracılığıyla STAT3'ün hedeflenmesi, kazanılmış ilaç direncini etkili bir şekilde tersine çevirmekte olup, dirençli KHDAK için uygulanabilir bir terapötik strateji temsil etmektedir.*

Anahtar Sözcükler: *Sisplatin direnci, hücre dışı veziküller, eksozomlar, KHDAK, STAT3*

INTRODUCTION

Lung cancer remains the leading cause of cancer-related mortality globally [1–4], with non-small cell lung cancer (NSCLC) accounting for approximately 85% of cases [5]. While platinum-based chemotherapeutic regimens, particularly cisplatin, serve as the cornerstone of first-line treatment [2,6], the clinical efficacy of these agents is frequently compromised by the development of acquired drug resistance. This resistance is multifactorial, involving increased drug efflux [7], enhanced DNA repair [8], and the activation of survival signaling pathways [9]. Among these pathways, the signal transducer and activator of transcription 3 (STAT3) has emerged as a critical oncogenic hub [10,11]. In resistant NSCLC, constitutive STAT3 activation promotes cell survival, inhibits apoptosis, and drives metastasis [12,13]. Consequently, silencing STAT3 expression—thereby dismantling this pro-survival signaling network—represents a potent therapeutic strategy to resensitize tumors to chemotherapy.

Despite the therapeutic promise of RNA interference (RNAi) technologies (small interfering RNAs abbreviated as siRNA, and short hairpin RNAs abbreviated as shRNA), their clinical translation is severely limited by delivery challenges [14]. Naked nucleic acids are rapidly degraded by serum nucleases, exhibit poor cellular uptake due to charge repulsion, and can trigger off-target immune responses. Furthermore, synthetic vectors such as cationic liposomes and polymers often exhibit cytotoxicity, are rapidly cleared by the reticuloendothelial system, and lack inherent tumor-specific targeting capabilities [15]. Consequently, the development of innovative and efficient delivery platforms for tumor-targeted nucleic acid therapeutics remains an ongoing necessity.

In recent years, extracellular vesicles (EVs)—particularly exosomes, which are nanovesicles approximately 30–150 nm in diameter—have gained significant attention as natural delivery systems [16,17]. Generated via the endosomal pathway, exosomes possess inherent advantages over synthetic carriers: they exhibit low immunogenicity, high circulatory stability, and the capacity to traverse biological barriers. The utilization of autologous EVs may further minimize immune rejection, enabling the development of personalized delivery platforms. Although the term 'exosome' is widely used, the latest MISEV 2023 guidelines emphasize that 'extracellular vesicle' is the preferred generic terminology. Because current purification methodologies often yield heterogeneous populations—encompassing vesicles budding directly from the plasma membrane alongside those of endosomal origin—assigning the specific term 'exosome' requires definitive proof of biogenesis [18]. Nevertheless, all EVs possess a unique molecular signature, comprising specific protein, lipid, and nucleic acid profiles dictated by their cell of origin [19]. Specifically, surface integrins and tetraspanins are canonical EV components that dictate tropism—the intrinsic ability of EVs to “home” to specific tissues and undergo internalization by designated recipient cells [16,20]. Notably, cancer-derived EVs possess a natural homing capacity toward

tumor sites, facilitated by their shared molecular identity with the parent cells [21–23].

In this study, we sought to leverage these intrinsic properties to overcome cisplatin resistance in NSCLC. We isolated EVs from the parental Calu-1 cell line and engineered them to deliver plasmid DNA encoding anti-STAT3 shRNA. We demonstrate that this biomimetic formulation effectively silences STAT3 expression, thereby restoring chemosensitivity in cisplatin-resistant lung cancer cells.

MATERIALS and METHODS

Cell culture

The human non-small cell lung cancer cell line Calu1 was obtained from the American Type Culture Collection (ATCC). Cells were cultured in Dulbecco's Modified Eagle Medium (DMEM) supplemented with 10% fetal bovine serum (FBS), 1% L-glutamine, and antibiotics. All cultures were maintained at 37°C in a humidified atmosphere containing 5% CO_2. To ensure the absence of contamination, routine mycoplasma testing was conducted using DAPI staining to visualize any extranuclear DNA. The cisplatin-resistant subline (CR-Calu-1) was established as described previously [24]. Briefly, parental Calu-1 cells were continuously exposed to stepwise increasing concentrations of cisplatin over several months until a stable resistant phenotype was achieved. Resistance was subsequently verified by determining the half-maximal inhibitory concentration (IC_{50}) via cell viability assays.

EV isolation

EVs were isolated from cell culture supernatants utilizing a modified differential ultracentrifugation protocol [25,26]. Briefly, Calu1 cells were cultured to 70–80% confluence, washed with PBS (pH 7.4), and incubated in exosome-depleted medium for 48-to-72 hours. The conditioned medium was subsequently collected and subjected to sequential centrifugation at 300 × g for 10 minutes and 2,000 × g for 20 minutes to eliminate dead cells and cellular debris. The resulting supernatant was then centrifuged at 10,000 × g for 30 minutes to deplete apoptotic bodies and larger microvesicles. To pellet the EVs, the clarified supernatant underwent ultracentrifugation at 120,000 × g for 90 minutes at 4°C using an Optima Max-XP ultracentrifuge (Beckman Coulter). The crude EV pellet was washed by resuspension in PBS and re-ultracentrifuged at 120,000 × g for an additional 90 minutes. Finally, the supernatant was discarded, and the purified EV pellet was resuspended in a minimal volume of PBS for immediate downstream applications.

Loading of shRNA-encoding plasmid into EVs

To achieve nucleic acid encapsulation, purified EVs were loaded with pDNA encoding either an anti-STAT3 short hairpin RNA (pSIH1-puro-STAT3 shRNA, abbreviated as pshSTAT3) or a control sequence (pSIH1-puro-control shRNA, abbreviated as pshControl) via lipofection-mediated membrane fusion, adapting a protocol previously described by Shtam et al. [27]. The shRNA sequence, encoded by the pshSTAT3 plasmid is gatccGCATCTGCCTAGATCGGCTATTCAAGAG ATAGCCGATCTAGGCAGATGTTTTTTg, and, the shRNA sequence, encoded by the pshControl plasmid is AATAGCGACTAAACACATCAATTCAAGAGATT GATGTGTTTAGTCGCTATTTTTTTT. The plasmids were a gift from Frank Sinicrope (Addgene plasmid #26596 and #26597, respectively) [28]. Prior to EV incubation, 500 ng of pDNA was pre-complexed with FuGENE HD transfection reagent in a total volume of 20 µL. To optimize loading efficiency, several transfection reagent-to-pDNA ratios were evaluated (0.6, 1.2, and 1.6 µL of FuGENE HD per 1 µg of pDNA), establishing 1.6 µL/µg as the optimal ratio. The resulting pre-complexes were subsequently combined with 30 µL of the purified EV suspension (equivalent to 900 ng of total EV protein) to yield a final ternary mixture volume of 50 µL. This formulation was incubated at room temperature to facilitate membrane fusion and biomimetic encapsulation.

Particle size and zeta potential analysis

Particle size distribution and zeta potential of the EV formulations were evaluated using a Zetasizer Nano ZS instrument (Malvern Panalytical, UK). Prior to measurement, all samples were diluted 20-fold with PBS. For particle size analysis via dynamic light scattering (DLS), and data were acquired in the backscatter mode at a detection angle of 173°. For zeta potential determination the samples were transferred into standard zeta potential capillary cells. Electrophoretic mobility was recorded and subsequently converted to zeta potential values using the Smoluchowski approximation.

Electron microscopy

Morphological characterization of the isolated EVs was performed using a field-emission scanning electron microscope (Zeiss Supra 40 VP, Oberkochen, Germany) operated in either scanning transmission electron microscopy (STEM) mode or standard scanning electron microscopy (SEM) mode equipped with an Everhart-Thornley detector. For STEM imaging, EV samples were adsorbed onto carbon-coated 400-mesh grids for 5 minutes. Excess buffer was wicked away using filter paper, and the samples were subsequently negatively stained with uranyl acetate. Images were acquired at an accelerating voltage of 20 kV at magnifications ranging from 50,000× to 145,000×. For SEM imaging, EV suspensions were deposited onto glass slides and allowed to dry. Prior to microscopy, the samples were sputter-coated with an approximately 5 nm layer of Au/Pd alloy to confer conductivity and minimize surface charging effects. SEM micrographs were obtained at an accelerating voltage of 5–7 kV and magnifications of 50,000× to 80,000×.

Atomic force microscopy (AFM)

Topographic characterization of the EVs was performed at the Ege University Central Research Test and Analysis Laboratory Application and Research Center (EGE-MATAL), adapting a protocol previously described by Shtam et al. [27]. Prior to analysis, glass slides were ultrasonically cleaned sequentially in ultrapure water and 99.5% ethanol for 30 minutes each, followed by air-drying. Freshly isolated EVs (5 µL) were deposited onto the prepared slides. Imaging was conducted using a Dimension Edge AFM/SPM system (Bruker Corp., Billerica, MA, USA) operated in tapping mode. Scans were acquired over a 5 × 5 µm area with a resolution of 512 × 512 pixels.

Protein quantification

Total protein concentration of the isolated EVs was determined using the Pierce Bradford Protein Assay Kit (Thermo Scientific, USA) according to the manufacturer's instructions. Briefly, 5 µL of each sample was pipetted into microplate wells in triplicate, followed by the addition of 150 µL of Bradford reagent. The plate was then incubated for 10 minutes at room temperature. Protein concentrations were calculated using a standard curve generated with bovine serum albumin (BSA) standards ranging from 5 to 25 µg/mL.

DNase I protection assay

To confirm the internal encapsulation of pDNA, the EV formulations were incubated with DNase I (1 U/µL) for 30 minutes at 37°C. The nucleolytic reaction was subsequently terminated by the addition of ethylenediaminetetraacetic acid. The protected DNA was then resolved and analysed via agarose gel electrophoresis. The visualization of intact plasmid bands was utilized to confirm successful encapsulation and protection against nuclease degradation.

In vitro cytotoxicity and re-sensitization studies

The cytotoxic effect of cisplatin on CR-Calu1 cells was evaluated using the WST-1 proliferation assay (Roche, USA). Briefly, cells were seeded into 96-well plates at a density of 3×10^3 cells per well. Following a 24-hour incubation period, the cells were treated with cisplatin at concentrations ranging from 50 to 300 µM prepared in DMEM supplemented with 4% FBS. All treatments were performed in triplicate. Cell viability was assessed at 48 and 72 hours post-treatment in accordance with the manufacturer's instructions. The IC_{50} of cisplatin was determined via variable slope non-linear regression using Equation 1:

$$Y = \frac{100}{1+10^{((logIC_{50}-X)\times HillSlope)}}$$

Equation 1

where X is the logarithm of the cisplatin concentration, Y is the normalized survival percentage, $logIC_{50}$ represents the logarithmic value of the cisplatin concentration corresponding to 50% cell death, and HillSlope is the unitless slope factor.

To evaluate the effect of the individual formulation components on cell proliferation, CR-Calu1 cells were treated with naked pshControl DNA, naked pshSTAT3 DNA, and blank EVs for 48 hours. Furthermore, to investigate the capacity of the engineered EVs to resensitize CR-Calu1 cells to cisplatin, the cells were divided into the following treatment groups: (i) free cisplatin, (ii) blank EVs + cisplatin, (iii) EV-loaded pshControl + cisplatin, and (iv) EV-loaded pshSTAT3 + cisplatin. Cell viability was measured at 48 hours post-treatment using the WST-1 assay. Absorbance values, obtained using a microplate reader, were normalized to the untreated control group to calculate the percentage of cell viability. All results

of this experiment were then normalized to the free cisplatin treatment to analyze the beneficial effect of the STAT3 expression silencing.

Reverse transcription-quantitative PCR (RT-qPCR)

Total RNA was isolated from treated CR-Calu1 cells using the MagNA Pure LC RNA Isolation Kit on a MagNA Pure LC automated extraction system (Roche), in accordance with the manufacturer's instructions. RNA concentration and purity were determined spectrophotometrically. First-strand cDNA was synthesized using the iScript cDNA Synthesis Kit (Bio-Rad) according to the manufacturer's protocol. Primer and probe sets for STAT3 and glyceraldehyde 3-phosphate dehydrogenase (GAPDH) were selected from the Universal Probe Library, and qRT-PCR analysis was performed using a LightCycler™ 480 instrument (both Roche). STAT3 mRNA expression levels were normalized to the endogenous reference gene GAPDH. Relative changes in gene expression were calculated using the standard $2^{-\Delta\Delta Ct}$ method.

Western blot

STAT3 protein expression was evaluated in CR-Calu1 cells across the identical treatment groups utilized for the mRNA expression analysis. Following 72 hours of treatment with the EV formulations, whole-cell lysates were prepared using the Complete Lysis-M Kit (Roche) according to the manufacturer's instructions. Briefly, cells were harvested via trypsinization, washed twice with cold PBS, and resuspended in lysis buffer. Following a 15-minute incubation under gentle agitation, the lysates were centrifuged at 22,000 × g for 15 minutes at 4°C. The clarified supernatant was collected, and total protein concentration was determined via the Bradford assay utilizing a bovine serum albumin (BSA) standard curve.

30 µg of total protein per lane were resolved by 8% sodium dodecyl sulfate-polyacrylamide gel electrophoresis (SDS-PAGE) and subsequently transferred onto polyvinylidene difluoride membranes using the iBlot Dry Blotting System (Invitrogen). The membranes were processed using a chromogenic western blot detection kit (Invitrogen) in accordance with the manufacturer's protocol. Membranes were probed with a primary antibody against STAT3 (1:1000 dilution) and a primary antibody against β-actin (1:1000 dilution). Following incubation with the appropriate species-specific secondary antibodies, protein bands were visualized via chromogenic detection.

Stability and lyophilization

To assess the clinical applicability and storage stability of the formulations, aqueous EV suspensions were stored at −20°C, 4°C, and 25°C for up to 3 months. Furthermore, to investigate the feasibility of long-term storage, EVs were lyophilized in the presence of various cryoprotectants (sucrose, trehalose, sorbitol, or glycine). Stock solutions of each cryoprotectant (10%) were prepared prior to use. To prepare the final formulations, EV suspension was mixed 1:1 or 1:3 (v/v) of the 10% cryoprotectant solution. The samples were mixed thoroughly and frozen overnight at −80°C. The samples were freeze-dried using FreeZone 6 instrument (Labconco, USA) for 24 hours at a pressure of 0.05 mbar. The obtained solid cakes were reconstituted with ultrapure water to the initial volume, and structural integrity was assessed via particle size analysis using DLS.

Statistical analysis

Unless otherwise specified, all experiments were performed in independent triplicates, and data are presented as the mean ± standard deviation (SD). Statistical comparisons between two independent groups were conducted using an unpaired Student's t-test. For multiple group comparisons, a one-way analysis of variance (ANOVA) followed by post-hoc Bonferroni's multiple comparison test, or a non-parametric Kruskal-Wallis test followed by Dunn's multiple comparisons test, was utilized as appropriate. Differences were considered statistically significant at $p < 0.05$.

RESULTS

Successful isolation and characterization of EVs

Morphological analyses utilizing SEM, STEM, and AFM confirmed that the isolated vesicles possessed the characteristic structure and morphology typical of extracellular vesicles (Figure-1). As depicted in Figures-1A, -1B, and -1D, the hydrodynamic size distribution of the EVs measured via DLS ranged from 100 to 500 nm, with the predominant population centering at ~300 nm. The average zeta potential was recorded between −28.6 and −25.5 mV (Figure-1C), indicating moderate colloidal stability. Total protein concentrations, as determined by the

Bradford assay, were 23.27 µg/mL and 31.81 µg/mL for EV samples isolated after 48 and 72 hours of incubation, respectively (Figure-1E). No statistically significant differences were observed in the physicochemical characteristics and the protein content of EVs isolated at these two time points. Notably, microscopic analyses revealed significantly smaller particle sizes compared to the DLS results (Figures-1F–1I). The mean particle sizes of samples isolated after 48 hours of incubation were 73.9 nm, 59.2 nm, and 134.7 nm, as measured by SEM, STEM, and AFM, respectively (Figure-1I).

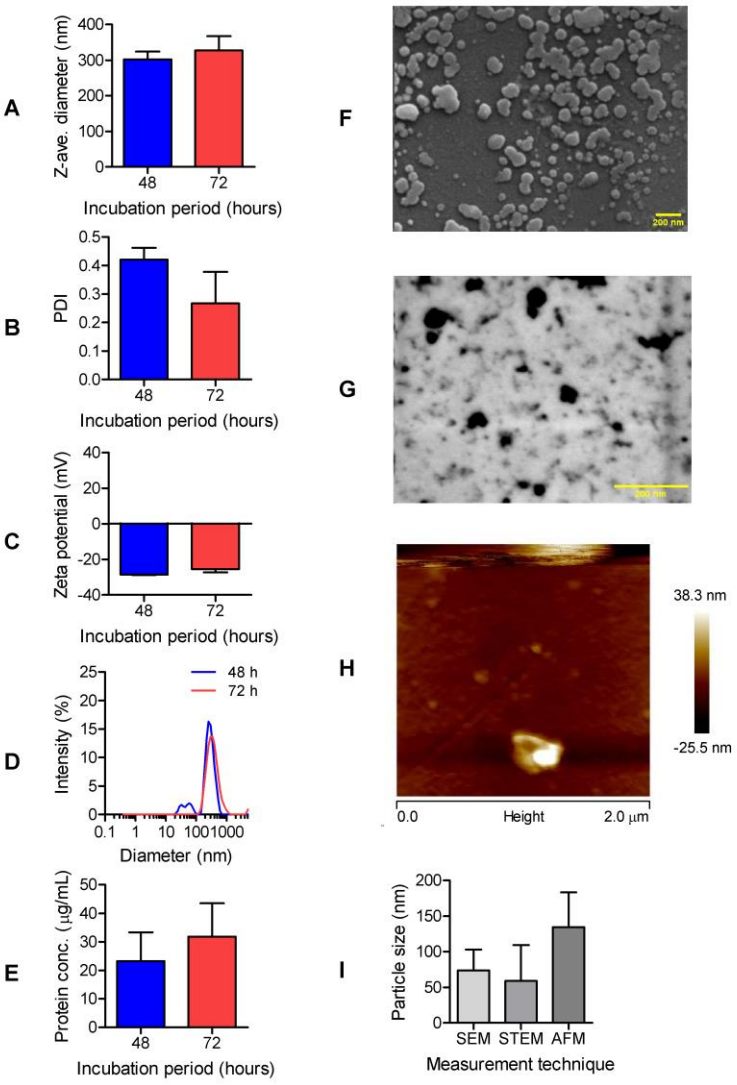

Figure-1: Characterization of EVs.
A: Particle size measured by DLS,
B: Polydispersity index,
C: Zeta potential,
D: Intensity-size distribution,
E: Protein concentration of EVs measured by BCA assay,
F: SEM image of EVs obtained after 48 h incubation, scalebar represents 200 nm,
G: STEM image of EVs obtained after 48 h incubation, scalebar represents 200 nm,
H: AFM topographic image of the EVs obtained after 48 h incubation,
I: Particle sizes of EVs according to the microscopic images. The AFM images yielded significantly larger particle size (SEM vs STEM $p>0.05$, SEM vs AFM $p<0.001$, STEM vs AFM $p<0.001$) as tested by a one way ANOVA followed by Bonferroni's multiple comparison test.

Plasmid DNA loading to the EVs

Agarose gel electrophoresis confirmed that the co-incubation of EVs with the pDNA-FuGENE pre-complexes resulted in successful plasmid association. Incomplete association was observed at a transfection reagent-to-pDNA ratio of 0.6 µL/µg, evidenced by the migration of a free pDNA band. Conversely, at elevated ratios of 1.2 and 1.6 µL/µg, the pDNA was fully complexed and retained within the loading wells (Figure-2A). The capacity of these ternary complexes (FuGENE HD:pDNA:EV) to release the associated plasmid was subsequently verified by incubating the formulations with 1% SDS prior to electrophoresis (Figure-2A). Morphological evaluation of the engineered EVs via SEM (Figure-2B) and STEM (Figure-2C) revealed a particle size of approximately 60 nm for both the pshControl-loaded and the pshSTAT3-loaded formulations. Furthermore, the ability of the EV formulation to shield the genetic payload from nuclease degradation was assessed using a DNase I protection assay. Agarose gel retardation analysis demonstrated that while naked pDNA was completely degraded by the endonuclease, the pDNA formulated within the EVs remained intact, displaying visible supercoiled bands (Figure-3).

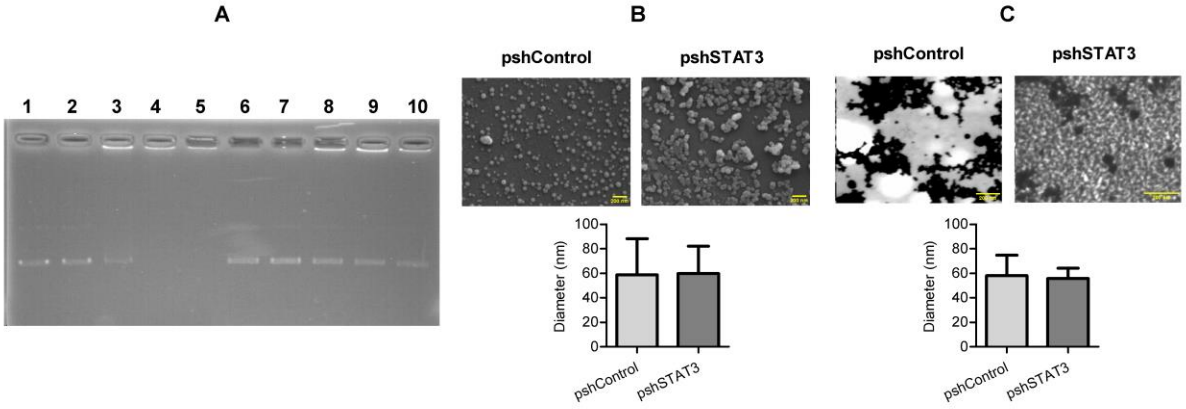

Figure-2. pDNA loading analysis and the characterization of EVs after lipofection. **A:** agarose gel retardation image of pDNA after lipofection of EVs with FuGene HD. Loading wells: 1- pDNA, 2- pDNA+EV, 3- FuGene: pDNA (0.6 µL/µg)+EV, 4- FuGene: pDNA (1.2 µL/µg)+EV, 5- FuGene: pDNA (1.6 µL/µg)+EV, 6- pDNA+SDS, 7- pDNA+EV+SDS, 8- FuGene: pDNA (0.6 µL/µg)+EV+SDS, 9- FuGene: pDNA (1.2 µL/µg)+EV+SDS, 10- FuGene: pDNA (1.6 µL/µg)+EV+SDS, **B:** SEM images of the pshControl- and pshSTAT3-loaded EVs. The bar graph represents the average particle size measured from the micrographs. Scale bar represents 200 nm, **C:** STEM images of the pshControl- and pshSTAT3-loaded EVs. The bar graph represents the average particle size measured from the micrographs. Scale bar represents 200 nm.

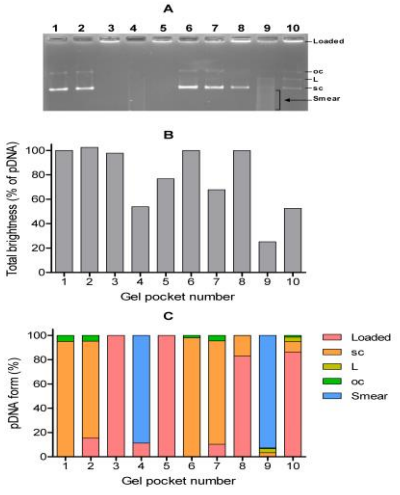

Figure-3. Analysis of the potential of FuGeneHD-transfected EVs to protect pDNA from nuclease activity.

A: Agarose gel photograph showing DNA bands following electrophoresis;
B: Densitometric analysis graph showing the total DNA fluorescence per well relative to the control pDNA-loaded well;
C: Densitometric analysis graph showing the percentages of pDNA topoisomers, complex-bound pDNA remaining in the well, and degraded pDNA forming a smear in each well. Loading wells:

1- pDNA,
2- pDNA+EV,
3- pDNA+FuGene+EV,
4- pDNA+DNaseI,
5- pDNA+FuGene+EV+DNaseI,
6- pDNA+SDS,
7- pDNA+EV+SDS,
8- pDNA+FuGene+EV+SDS,
9- pDNA+DNaseI+SDS,
10- pDNA+FuGene+EV+DNaseI+SDS.

Abbreviations: oc: open circular form, L: linear form, sc: super coil form

STAT3 silencing reverses cisplatin resistance

Initial cell viability assays confirmed that CR-Calu-1 cells exhibited significant resistance to cisplatin compared to the parental cell line (IC_{50} > 190 µM) (Figures-4A and -4B). Neither the naked plasmids nor the blank EVs alone induced measurable cytotoxicity in the CR-Calu-1 cells (Figure-4C). Treatment of these resistant cells with the pshSTAT3-loaded EV formulation resulted in a significant reduction in STAT3 mRNA levels (a 48% reduction as a monotherapy, and a 58% reduction when combined with cisplatin) compared to untreated controls (Figure-4D). Western blot analysis corroborated these transcriptional findings, demonstrating a marked decrease in STAT3 protein expression (Figure-4E). While blank EVs had no effect on cell viability, and the pshControl-loaded EVs combined with cisplatin caused moderate growth inhibition, the combination of pshSTAT3-loaded EVs and cisplatin resulted in a synergistic cytotoxic effect observed across three sub-IC50 doses (Figure-4F). Specifically, at cisplatin concentrations of 50, 100, and 150 µM, the viability of CR-Calu1 cells was reduced to 67.6%, 53.7%, and 59.1%, respectively, relative to the free cisplatin-treated group.

p<0.01, * p<0.05.

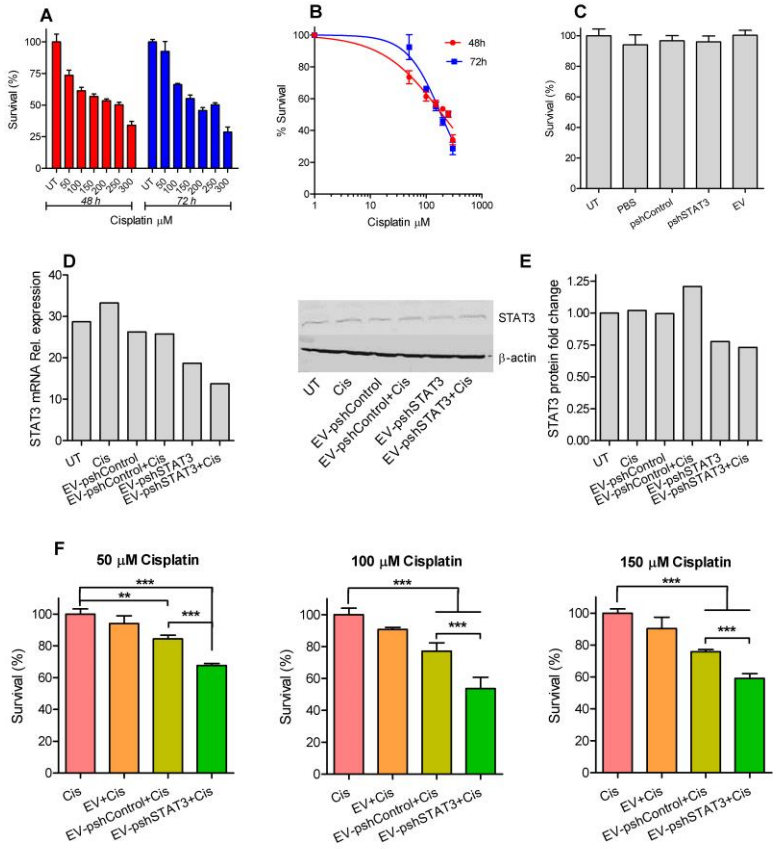

Figure-4. Efect of the shSTAT3-loaded EVs on the cisplatin resistant NSCLC cells.
A: Cell viability of CR-Calu1 cell line exposed to different doses of cisplatin. Cell survival percentage is normalized against the untreated control;
B: Non-linear regression analysis of the dose-response.
C: Effect of the blank EVs and the plasmids-alone on the CR-Calu1 cells.
D: Relative expression of STAT3 mRNA after treatment of the CR-Calu1 cells with shSTAT3-encoding plasmids loaded to EVs;
E: Fold change in the STAT3 protein level by Western blot analysis after treatment of the CR-Calu1 cells with shSTAT3-encoding plasmids loaded to EVs;
F: Effect of the STAT3 silencing by shSTAT3-loaded EVs on the cisplatin response of CR-Calu1 cells. Cell survival is normalized against the cisplatin-alone group and presented as percentage. All treatments were performed in triplicate. *** p<0.001, **

Stability and lyophilisation

Stability studies revealed that aqueous EV suspensions stored at −20°C suffered from pronounced aggregation and membrane fusion, likely induced by ice crystal formation. Storage at 4°C successfully preserved the initial size characteristics for up to two weeks. Conversely, storage at room temperature (25°C) resulted in a significant increase in particle size, indicative of progressive vesicle instability (Figure-5). To ensure long-term preservation, lyophilisation conditions were optimized. Representative macroscopic images detailing the physical appearance of the lyophilized cakes alongside post-reconstitution size measurement data are presented in Figure-6. Among the formulations tested, 7.5% glycine proved superior. EVs freeze-dried in the presence of 7.5% glycine retained a mean hydrodynamic diameter of ~300 nm upon reconstitution, successfully circumventing the aggregation observed in unprotected control samples and those formulated with the other excipients. Furthermore, the 7.5% glycine formulation yielded structurally well-formed macroscopic cakes compared to the alternative cryoprotectants. In contrast, sorbitol, trehalose, and sucrose were less effective at preventing aggregation, resulting in notable increases in both particle size and polydispersity.

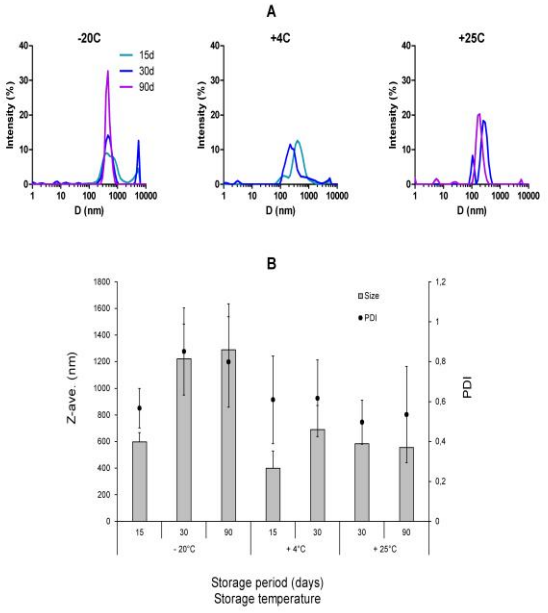

Figure-5. Storage stability of the EVs.
A: Intensity-size distribution plots of the EVs stored at different temperatures,
B: Bar graph showing the average hydrodynamic size and the polydispersity of the EVs.

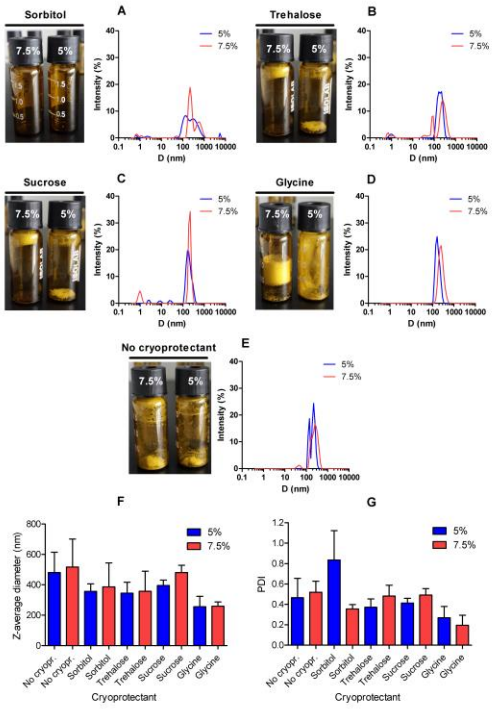

Figure-6. Characteristic properties of the lyophilized EV samples. In sections A-E, a representative picture showing the appearance of the lyophilized EVs, and the intensity-size distribution plots of the samples after the rehydration measured by DLS are provided. Results of samples with
A: sorbitol,
B: trehalose,
C: sucrose,
D: glycine as a cryoprotectant,
E: results of samples with no cryoprotectant,
F: Bar graph demonstrating the Z-average particle size of the lyophilized samples;
G: Bar graph demonstrating the polydispersity of the lyophilized samples. All cryoprotectants were tested at 5% and 7.5% final concentration.

DISCUSSION

The broad size distribution observed is consistent with the inherent heterogeneity of EVs [18]. The well-documented discrepancy in particle size between characterization methods is primarily attributed to the measurement environment [29,30]. DLS measures the hydrodynamic diameter of particles suspended in a liquid dispersion, which inherently includes the surrounding hydration layer. Conversely, microscopic methods require sample dehydration prior to imaging; thus, the hydration layer is lost, and the vesicles undergo structural shrinkage, yielding smaller recorded particle sizes.

Regarding pDNA loading, the gel retardation findings confirm the successful internal

encapsulation of the plasmid within the EVs, conferring robust protection against extracellular nucleolytic degradation.

In viability assays, the resistance of CR-Calu-1 cells was consistent with our previous observations [24]. It is important to note that the control plasmid also induced a slight reduction in cell growth compared to untreated cells, which may be attributed to a non-specific cellular response to exogenous nucleic acids. Nevertheless, the pshSTAT3-loaded EVs reduced cell survival in a statistically significant manner compared to the control shRNA, demonstrating that silencing STAT3 expression actively restores the sensitivity of resistant cells to cisplatin. The development of drug resistance in NSCLC is a complex biological hurdle, often necessitating the blockade of compensatory survival pathways such as STAT3 [12]. While the biological rationale for targeting STAT3 is robust, the effective delivery of RNAi therapeutics remains a major barrier in gene therapy. This study addresses this critical challenge by utilizing an extracellular vesicle-based delivery vector. Our results demonstrate a clear and significant resensitization effect. The EVs functioned as a biomimetic nanocarrier, effectively shielding and delivering the shRNA plasmid into the resistant cells. The subsequent knockdown of STAT3 likely destabilized the pro-survival signalling network, rendering the cells vulnerable to cisplatin-induced cytotoxicity. Furthermore, the successful utilization of Calu1-derived EVs to treat resistant Calu1 cells suggests that an autologous therapeutic approach—harvesting EVs from a patient's tumor cells, loading them with therapeutic cargo, and re-administering them—represents a promising conceptual approach that may significantly enhance targeted cellular uptake due to homologous surface marker recognition, though this requires rigorous in vivo confirmation.

While trehalose is frequently reported in the literature to provide optimal cryopreservative effects for biological vesicles [31–33], our findings diverged from these observations. This discrepancy is most likely attributable to differences in the EV cellular source—which dictates inherent membrane lipid composition—as well as the specific cryoprotectant concentrations utilized in this study. A major translational bottleneck for EV-based therapeutics is long-term storage, as aqueous EV suspensions are prone to rapid degradation and aggregation. Our identification of 7.5% glycine as an effective cryoprotectant represents a vital step toward clinical applicability. Mechanistically, glycine likely functions by replacing water molecules at the vesicle surface and acting as a protective bulking agent, thereby maintaining the structural integrity of the lipid bilayer during the physical stress of the lyophilization process. Recently, it was reported that a combination of 5% trehalose, 5% mannitol, and 2.5% glycine effectively protected the structural integrity, protein content, and biomarker expression of milk-derived EVs during storage [34]. Future investigations should explore similar multi-component cryoprotectant combinations to further optimize the preservation of EV therapeutics. Furthermore, while the immediate post-reconstitution integrity of the lyophilized EVs was confirmed in this study, the long term shelf-life of these solid formulations was not evaluated. Therefore, future studies must also assess the long-term storage stability of the lyophilized EV cakes.

While the findings presented herein are highly promising, this study is inherently limited by its reliance on an *in vitro* 2D cell culture model. The high complexity of the tumor microenvironment, alongside the *in vivo* pharmacokinetics, biodistribution, and systemic clearance of the engineered EVs, necessitates comprehensive validation in appropriate animal models. Additionally, despite rigorous differential ultracentrifugation, the isolated EV population retains an inherent degree of biological heterogeneity (comprising a mixture of endosomally-derived nanovesicles and plasma membrane-derived microvesicles). Future investigations incorporating advanced downstream purification techniques, such as size-exclusion chromatography or density gradient centrifugation, could further refine and standardize the formulation.

CONCLUSION

In conclusion, we have successfully engineered a functional, stable, and highly effective EV-based gene delivery platform. By encapsulating plasmid DNA encoding anti-STAT3 shRNA into lung cancer-derived EVs, we effectively bypassed the delivery limitations of naked nucleic acids and reversed acquired cisplatin resistance *in vitro*. Furthermore, the successful lyophilization of this formulation addresses a major translational storage hurdle. While these *in vitro* findings

provide a strong foundation for developing stable allogeneic preparations and autologous EV therapies for refractory non-small cell lung cancer, comprehensive EV characterization and *in vivo* validation remain essential next steps toward clinical translation.

Conflict of Interest: The authors declare that there is no real, potential, or perceived conflict of interest for this article.

Acknowledgements: This study was funded by the Scientific and Technological Research Council of Türkiye (TÜBİTAK) (Project Number: 115S829 to MK). The authors also acknowledge the use of analytical instrumentation at the Pharmaceutical Sciences Research Laboratory (FABAL), Ege University Faculty of Pharmacy, supported by the Republic of Türkiye Ministry of Development (Infrastructure Project #2009K120640).

References

1. Shong LY-W, Lam DC-L. Emerging trends in global lung cancer burden. Semin Respir Crit Care Med 2025;46(5):409-18.
2. Jeon H, Wang S, Song J, Gill H, Cheng H. Update 2025: Management of non-small-cell lung cancer. Lung 2025;203(1):53.
3. Siegel RL, Kratzer TB, Giaquinto AN, Sung H, Jemal A. Cancer statistics, 2025. CA Cancer J Clin 2025;75(1):10-45.
4. Ji Y, Zhang Y, Liu S, et al. The epidemiological landscape of lung cancer: Current status, temporal trend and future projections based on the latest estimates from GLOBOCAN 2022. J Natl Cancer Cent 2025;5(3):278-86.
5. de Alencar VTL, Formiga MN, de Lima VCC. Inherited lung cancer: A review. Ecancermedicalscience 2020;14:1008.
6. Bouchard N, Daaboul N. Lung cancer: Targeted therapy in 2025. Curr Oncol 2025;32(3):146.
7. Chen Z, Shi T, Zhang L, et al. Mammalian drug efflux transporters of the ATP binding cassette (ABC) family in multidrug resistance: A review of the past decade. Cancer Lett 2016;370(1):153-64.
8. Manguinhas R, Serra PA, Gil N, Rosell R, Oliveira NG, Guedes RC. Novel DNA repair inhibitors targeting XPG to enhance cisplatin therapy in non-small cell lung cancer: Insights from in silico and cell-based studies. Cancers 2024;16(18):3174.
9. Duan S, Tsai Y, Keng P. IL-6 signaling contributes to cisplatin resistance in non-small cell lung cancer via the up-regulation of anti-apoptotic and DNA repair associated molecules. Oncotarget 2015;6(29):27651-60.
10. Dutta P, Sabri N, Li J, Li WX. Role of STAT3 in lung cancer. JAKSTAT 2014;3(4):e999503.
11. Mohrherr J, Uras IZ, Moll HP, Casanova E. STAT3: Versatile functions in non-small cell lung cancer. Cancers 2020;12(5):1107.
12. Sun C-Y, Nie J, Huang J-P, Zheng G-J, Feng B. Targeting STAT3 inhibition to reverse cisplatin resistance. Biomed Pharmacother 2019;117:109135.
13. Morelli AP, Tortelli TC, Mancini MCS, et al. STAT3 contributes to cisplatin resistance, modulating EMT markers, and the mTOR signaling in lung adenocarcinoma. Neoplasia 2021;23(10):1048-58.
14. Kotmakçı M, Çetintaş VB, Kantarcı AG. Preparation and characterization of lipid nanoparticle/pDNA complexes for STAT3 downregulation and overcoming chemotherapy resistance in lung cancer cells. Int J Pharm 2017;525(1):101-11.
15. Liu C, Zhang L, Zhu W, et al. Barriers and strategies of cationic liposomes for cancer gene therapy. Mol Ther Methods Clin Dev 2020;18(11):751-64.
16. Sen S, Xavier J, Kumar N, Ahmad MZ, Ranjan OP. Exosomes as natural nanocarrier-based drug delivery system: Recent insights and future perspectives. 3 Biotech 2023;13(3):101.
17. Ebrahimi F, Kumari A, Ghadami S, Al Abdullah S, Dellinger K. The potential for extracellular vesicles in nanomedicine: A review of recent advancements and challenges ahead. Adv Biol 2025;9(8):2400623.
18. Welsh JA, Goberdhan DCI, O'Driscoll L, et al. Minimal information for studies of extracellular vesicles (MISEV2023): From basic to advanced approaches. J Extracell Vesicles 2024;13(2):e12404.
19. Carvalho Ferraz L, Pereira P, Ferreira JV. Molecular mechanisms of extracellular vesicle biogenesis and their impact on the design of custom EVs. Adv Healthc Mater 2025;14:2501349.
20. Hoshino A, Costa-Silva B, Shen TL, et al. Tumour exosome integrins determine organotropic metastasis. Nature 2015;527(7578):329-35.
21. Cheng X, Henick BS, Cheng K. Anticancer therapy targeting cancer-derived extracellular vesicles. ACS Nano 2024;18(9):6748-65.
22. Sancho-Albero M, Decio A, Akpinar R, et al. Melanoma extracellular vesicles membrane coated nanoparticles as targeted delivery carriers for tumor and lungs. Mater Today Bio 2025;30:101433.
23. Zhou X, Miao Y, Wang Y, et al. Tumour-derived extracellular vesicle membrane hybrid lipid nanovesicles enhance siRNA delivery by tumour-homing and intracellular freeway transportation. J Extracell Vesicles 2022;11(3):e12198.

24. Cetintas VB, Kucukaslan AS, Kosova B, et al. Cisplatin resistance induced by decreased apoptotic activity in non-small-cell lung cancer cell lines. Cell Biol Int 2012;36(3):261-5.
25. Kotmakçı M, Erel Akbaba G. Exosome isolation: Is there an optimal method with regard to diagnosis or treatment? In: Wang J (ed). Novel implications of exosomes in diagnosis and treatment of cancer and infectious diseases. InTech; 2017:163-82.
26. Ohno S, Takanashi M, Sudo K, et al. Systemically injected exosomes targeted to EGFR deliver antitumor microRNA to breast cancer cells. Mol Ther 2013;21(1):185-91.
27. Shtam TA, Kovalev RA, Varfolomeeva EY, Makarov EM, Filatov MV. Exosomes are natural carriers of exogenous siRNA to human cells *in vitro*. Cell Commun Signal 2013;11(1):88.
28. Huang S, Sinicrope FA. Sorafenib inhibits STAT3 activation to enhance TRAIL-mediated apoptosis in human pancreatic cancer cells. Mol Cancer Ther. 2010; 9(3):742-50.
29. Wilson BK, Prud'homme RK. Nanoparticle size distribution quantification from transmission electron microscopy (TEM) of ruthenium tetroxide stained polymeric nanoparticles. J Colloid Interface Sci 2021;604:208-20.
30. Lai JJ, Chau ZL, Chen SY, et al. Exosome processing and characterization approaches for research and technology development. Adv Sci 2022;9(15):2103222.
31. Charoenviriyakul C, Takahashi Y, Nishikawa M, Takakura Y. Preservation of exosomes at room temperature using lyophilization. Int J Pharm 2018;553(1):1-7.
32. Neupane YR, Huang C, Wang X, et al. Lyophilization preserves the intrinsic cardioprotective activity of bioinspired cell-derived nanovesicles. Pharmaceutics 2021;13(7):1052.
33. Bosch S, de Beaurepaire L, Allard M, et al. Trehalose prevents aggregation of exosomes and cryodamage. Sci Rep 2016;6(1):36162.
34. Nathani A, Padakanti SC, Bagde A, Singh M. Long-term stabilization of non-bovine milk exosomes using lyophilization: Toward oral delivery of PROTAC therapeutics. J Drug Deliv Sci Technol 2026;115:107821.